Hollow-Core Photonic Band Gap Fibers for Particle Acceleration

Robert J. Noble and James E. Spencer
SLAC National Accelerator Laboratory
2575 Sand Hill Road, Menlo Park, CA 94025, USA

Boris T. Kuhlmey
Centre for Ultrahigh-bandwidth Devices for Optical Systems,
School of Physics, University of Sydney,
Sydney, New South Wales 2006, Australia

Abstract

Photonic band gap (PBG) dielectric fibers with hollow cores are being studied both theoretically and experimentally for use as laser driven accelerator structures. The hollow core functions as both a longitudinal waveguide for the transverse-magnetic (TM) accelerating fields and a channel for the charged particles. The dielectric surrounding the core is permeated by a periodic array of smaller holes to confine the mode, forming a photonic crystal fiber in which modes exist in frequency pass-bands, separated by band gaps. The hollow core acts as a defect which breaks the crystal symmetry, and so-called defect, or trapped modes having frequencies in the band gap will only propagate near the defect. We describe the design of 2-D hollow-core PBG fibers to support TM defect modes with high longitudinal fields and high characteristic impedance. Using as-built dimensions of industrially-made fibers, we perform a simulation analysis of the first prototype PBG fibers specifically designed to support speed-of-light TM modes.

1 Introduction

Due to electrical breakdown of metals in the presence of high electric fields, conventional particle accelerators, which consist of metal cavities driven by high-power microwaves, typically operate with accelerating fields of 20 to 40 mega-volts/meter (MV/m). Charged particle devices are often large and expensive due to the accelerator length and total stored energy needed to achieve high energy. Size and cost reductions are required for many applications. By comparison, the maximum surface fields of dielectric materials exposed to pulsed laser light are fluence-limited to the order of

a joule/cm^2 below 2 pico-second pulse lengths and are expected to exceed 10^9 volts/meter (gigavolt/meter = GV/m) [1]. These fields are an order of magnitude above metallic structures, making a laser-powered, dielectric waveguide an attractive medium for particle acceleration [2, 3, 4].

Transverse magnetic (TM) modes are used for particle acceleration and are so named because they have a longitudinal electric field on the accelerator axis and no longitudinal magnetic field on axis. To achieve particle acceleration in the absence of conducting boundaries, a dielectric structure must be designed which will support a TM mode with a uniform longitudinal electric field, slow the accelerating wave's phase velocity to be synchronous with the relativistic particle ($v \approx c$), and confine the field energy near the particle beam. The refractive index of dielectrics like silica (SiO2) is greater than one and will naturally reduce the wave phase velocity $v_p = c/n_{eff} = \omega/k_z$. Here c is the speed of light, n_{eff} is the mode's effective index, k_z is the propagation constant (wavenumber) in the material, $\omega = ck_0 = 2\pi c/\lambda$ is the frequency, and λ is the free-space wavelength. Silica is highly resistant to radiation damage, has a damage threshold of about 2 GV/m at a picosecond [1], and is transmissive from 0.2 to 2.1 microns [5], making this the natural wavelength range for an optical particle accelerator. Optical fiber technology is well developed and adaptable to drawing dielectric waveguides in the form of an accelerator. Efficient pulsed lasers have been developed by the telecommunications industry for these wavelengths so power sources are also available.

Field confinement without metal boundaries can be achieved by optical interference through the creation of a so-called photonic crystal, a dielectric structure arranged in a periodic geometry [6, 7]. Solutions to Maxwell's equations in a periodic system must exhibit the underlying symmetry of the periodic array, and allowed modes are those which scatter coherently from the distributed inclusions. This results in frequency pass-bands and stop-bands through constructive and destructive interference. The electromagnetic modes of a photonic crystal lie in a set of allowed bands, and it will similarly exhibit one or more photonic band gaps (stop-bands). The frequencies in the gap correspond to modes with periodicity unmatched to the lattice and hence unable to propagate. The PBG structure acts like a perfectly reflecting mirror at these frequencies. Trapped modes, also referred to as defect modes in optics terminology, can be obtained by breaking the symmetry with the introduction of a defect into the lattice. Since modes at the band gap frequencies are forbidden to propagate in the crystal, these are spatially confined to the defect region and are evanescent in the extended crystal. In this paper we consider two-dimensional (2-D) photonic band gap (PBG) fibers similar to the holey fibers motivated many years ago for long-haul telecommunications [8], and today used for high-power pulse delivery, gas-optic, and opto-fluidic experiments. The longitudinal defect in a 2-D PBG fiber acts as an optical waveguide with trapped modes propagating along the axis. For telecom or pulsed power transport, the defect confines TEM-like (transverse electric-magnetic) modes in the air core to minimize absorption loss, and dB/km losses have been demonstrated [9]. For an accelerator the central hole simultaneously provides a clear path for charged particles as well as an optical waveguide for the TM mode.

PBG confinement of TM modes for particle acceleration was first described by Kroll et al [10] in 11 GHz radio frequency (rf) structures composed of sapphire and metallic boundaries. The combined advantages of slow-wave confinement and gigavolt per meter gradients in all-dielectric structures led to the proposal by X.E. Lin to form an accelerator with a single glass fiber permeated by a lattice of vacuum holes surrounding a central defect hole of larger diameter [4]. The geometry

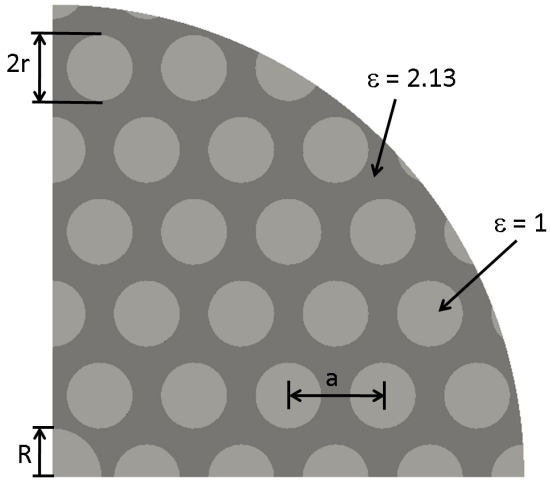

Figure 1: Quarter cross section of the Lin PBG structure, consisting of a lattice of vacuum holes (white) in a glass substrate (gray) with lattice period a and hole radii $r = 0.35a$. The periodic lattice holes serve to confine the accelerating mode, and the particle beam is accelerated within the central defect, radius $R = 0.52a$, propagating perpendicular to the page.

of the original Lin concept is shown in a quarter cross-section in Fig. 1. The operating frequency of the accelerator lies inside a band gap crossing the light line near $k_z a = 8.2$ (lattice period a), which is illustrated in Fig. 2. In this figure, the interior regions enclosed by the colored lines are band gaps, and outside of these are the regions where modes of the perfect crystal can freely propagate. The defect size is tuned to give a trapped TM mode in the center of the band gap with a dispersion relation crossing the light line. In this special case, the phase velocity equals the speed of light (SOL), giving rise to the nomenclature TM SOL mode.

Fiber accelerator design is generally very different from that for telecommunication fibers in which a confined TEM-like mode is desired, and other modes are suppressed by design of the fiber defect region. Another difference is the length of continuous fiber needed. A fiber accelerator will be made up of many short sections, most likely integrated with laser input couplers on a micro-fabricated chip. The accelerator section length L is determined by the time duration it takes the particle bunch moving near c to slip past the wave packet with its lower group velocity, $L = cv_g\tau_p/(c - v_g)$. The pulse length τ_p is about 10^{-12} sec consistent with the damage limit at 1 micron wavelength, and the fiber group velocity v_g is typically about $0.6c$, implying a length of 450 microns. Hence our accelerator sections are envisioned to be of order a millimeter long, each producing about 1 MeV energy gain, after which a re-phasing must occur between the particle bunch and the laser pulse.

This paper will focus on numerical simulations of fiber TM modes, the design of the defect and surrounding matrix to obtain an efficient accelerating mode, and the analysis of as-built prototype fibers. Our scope is limited to the electromagnetic properties of the PBG accelerating modes without consideration for input power coupling [11] and beam-interaction issues [12], both of which are parallel works in progress. We use a publicly available code based on the multipole

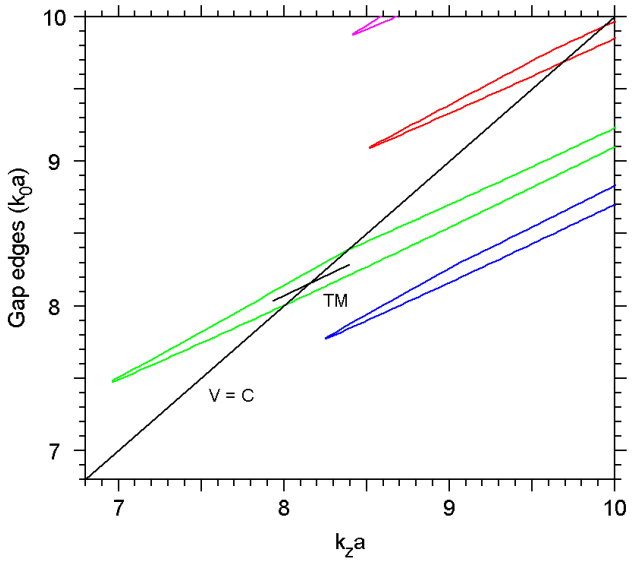

Figure 2: The lowest band gaps near the light line (v=c) for the Lin fiber plotted on the frequency-wavenumber dispersion plane as calculated with BandSolve. When a defect hole of the correct size is introduced, a TM mode with dispersion line crossing the light line appears in the band gap.

method [13] as well as the commercial software BandSolve from R-Soft [14] for the simulations. The multipole method uses Fourier-Bessel expansions centered on each fiber hole and solutions matched at the vacuum-dielectric boundaries [15]. The multipole method has frequency as the input parameter, which is supplied as the free-space wavelength $\lambda = 2\pi c/\omega$. The code searches for modes with different propagation constants (longitudinal wave number as distinguished by different n_{eff}) at this frequency within a specified range. The code generally searches for modes with complex propagation constants, the imaginary part accounting for longitudinal attenuation of the leaky mode as power diffracts transversely from the finite-layer fiber. The R-Soft BandSolve code uses a plane-wave expansion [16] to solve for fiber eigenmodes on a super-cell lattice with periodic boundary conditions. In fact what is mathematically calculated is a periodic array of defects, and with a large enough supercell, this geometry approximates an isolated defect. Provided that the supercell is large enough so the field cross-talk at the edges is limited, the defect modes can be faithfully calculated. This is verified by repeating the calculation with supercells of different sizes and comparing the results. This feature of the code can be exploited to explore multi-defect fibers which have been proposed for so-called parallel or lattice-beam accelerators [17]. We have also used the multipole method to calculate the accelerating modes of multi-defect fibers, and this will be discussed in a future publication.

The studies reported here are motivated to improve our understanding of the physics of acceleration modes in PBG fibers, inform the engineering and fabrication by our industrial partner of micron-scale, capillary fibers for relativistic electron acceleration, and to calculate the mode spectrum of commercial telecom fibers that will be used in our first beam-driven, wake-field experiments. Recently the first prototype fibers designed to support TM modes in the range of 4-8

microns were successfully made through our collaboration with Incom Inc. [18] The manufacture of TM-mode fibers operating in the range of 1- 2 microns wavelength is in progress. The different fibers are being tested with an electron beam as part of the ongoing experimental program to develop all-dielectric, compact laser accelerators at the SLAC National Accelerator Laboratory [12]. A detailed exposition of the engineering, fabrication, and beam testing of these fibers will be the subject of a forthcoming publication.

The remainder of this paper is organized as follows. In section 2, we introduce the reader to the special properties of TM modes near the light line in hollow-core fibers. The fiber geometry proposed by X.E. Lin [4] is employed as an example. These theoretical fiber dimensions are the starting point for our design of borosilicate prototypes fabricated by our industrial partner, Incom Inc., but with modifications intended to increase the acceleration gradient and reduce the high fields that can damage the glass. In section 3, we present a numerical analysis of the first prototype TM fibers drawn to micron-scale dimensions by Incom and discuss our simulation results. In section 4 we show how to significantly improve the accelerating mode properties of a hollow-core fiber by modifying the defect, adjusting the hole radii in the first layer, and adding small capillaries to the lattice. In section 5, we discuss the TM modes in commercial telecommunication fibers and give an example of a TM mode predicted in R-Soft/BandSolve simulations. This mode can be generated in wake-field experiments when a relativistic beam passes down the fiber core, thus serving as a calibration of the codes. A summary of the results is given in the last section.

2 Transverse Magnetic Defect Mode in PBG Fiber

2.1 Key Parameters and Mode Properties

The three basic requirements for a traveling wave particle accelerator are a longitudinal electric field on axis (electric field parallel to particle velocity vector), synchronization of particle and wave phase velocity, and confinement of field energy. The first two are needed to insure energy transfer to the particle over long distances. The final requirement is one of efficiency, insuring that input power overlaps strongly with the region where particles will absorb energy and be accelerated. As discussed in the Introduction, a TM-like SOL mode is necessary for relativistic particle acceleration. The dielectric structure must be designed to support a confined mode with a high longitudinal field on axis, called the acceleration gradient G, and a low stored power P. There will always be a maximum field E_{max} in the structure where breakdown damage will occur, and the structure is designed with as large a ratio of G/E_{max} as possible. The usual accelerator figure of merit relating gradient to stored power is defined by the so-called characteristic impedance, $Z_c = G^2\lambda^2/P$, where λ is the mode wavelength. This is the square of the voltage gain in one wavelength divided by the mode stored power, following the conventional electric circuit analogy.

Design of a two-dimensional PBG fiber for particle acceleration involves a specification of both the lattice and the defect. Since the transverse confinement of the accelerating mode is due to an interference effect over many lattice layers, the transverse scale of the structure is many

wavelengths. This is a major design difficulty compared to a metallic structure, which is typically only about a wavelength in size transversely. The fiber fields are spread out over a large area which must be accurately simulated, and the fields are subject to perturbations in the surrounding matrix. Two of the most serious effects of perturbations are to change the wavelength and phase velocity of a wave (driven at a fixed frequency), which leads to loss of synchronous acceleration, and to cause modes to radiate. Mode confinement is never perfect as this would require an infinite number of lattice layers. The finite number of layers gives rise to transverse diffraction of light out of the fiber at the boundary and decay of the Poynting flux. For long hollow core fibers, it is now understood that the main source of power loss is scattering from imperfections at the surface of the hollow core, because of the surface roughness originating from capillary waves frozen in during the drawing process [19]. This is less of a problem over a millimeter accelerator section where geometric dimensions are essentially constant in the draw, and usually diffractive power loss is the main problem. Power loss due to material absorption is no longer an issue in pure silica fibers. Modern fibers operate at the silica clarity limit of $< 1\ dB/km$ in the 1-2 micron range, which is determined by absorption and scattering loss on SiO2 molecules, described by Rayleigh scattering ($\sim \lambda^{-4}$) [20]. As a result, kilowatt average power is now routine in fibers.

For a simple round-hole, hexagonal lattice, the four constants that determine the PBG geometry are the transverse hole spacing or lattice period, a, which sets the scale of the system, the ratio of hole radius to lattice spacing, r/a, the ratio of central defect radius to lattice spacing, R/a, and the relative permittivity (dielectric constant) of the matrix, ϵ_r. Due to the high degree of symmetry, hexagonal lattices exhibit the widest band gaps (good mode separation) compared to other regular lattices, and their natural close-packing makes them the simplest array to manufacture. The band diagram in dimensionless units of ka is determined by the ratio r/a and the permittivity. Generally as the relative amount of dielectric increases (smaller air holes) or the permittivity increases (higher ϵ_r), the bands shift lower in frequency with the band diagram consisting of several well separated gaps at relatively smaller values of $k_0 a = \omega a/c$. The group velocity of modes also decreases with smaller holes and higher permittivity. The theoretical fiber of X.E. Lin [4] discussed in the Introduction is an example with about half the matrix volume being glass, as shown in Fig. 1. In this case, the particular hole size $r/a = 0.35$ was chosen so that a band-gap crosses the light-line at about the point where the gap is the widest, which generally improves mode confinement (Fig. 2).

The defect hole radius R is specifically chosen so that a TM-like defect mode crosses the light-line near the center of the band gap, insuring good confinement and mode separation. When the defect of size $R/a = 0.52$ is introduced, the accelerating mode shown in Figure 3 resides in the bandgap crossing the light line near $k_0 a \simeq 8.2$, corresponding to $\lambda = 0.77a$. For example, the choice of lattice spacing $a = 1.3\ \mu m$ yields an accelerating mode with a wavelength $\lambda = 1\mu$m. This mode is reasonably efficient for acceleration with an impedance $Z_c = 19\ \Omega$, an axial gradient to maximum field ratio $G/E_{max} = 0.48$, and a group velocity of 0.58c. This is the smallest defect size for which a TM mode appears in this gap. A larger defect would be better for beam transport, but as the defect size increases the TM mode shifts to higher frequency and out of the gap. New TM modes may enter the band gap from below, but they will typically have lower characteristic impedance and gradient for reasons we discuss next.

The longitudinal and radial electric field intensities are shown in Fig. 3 for the defect mode

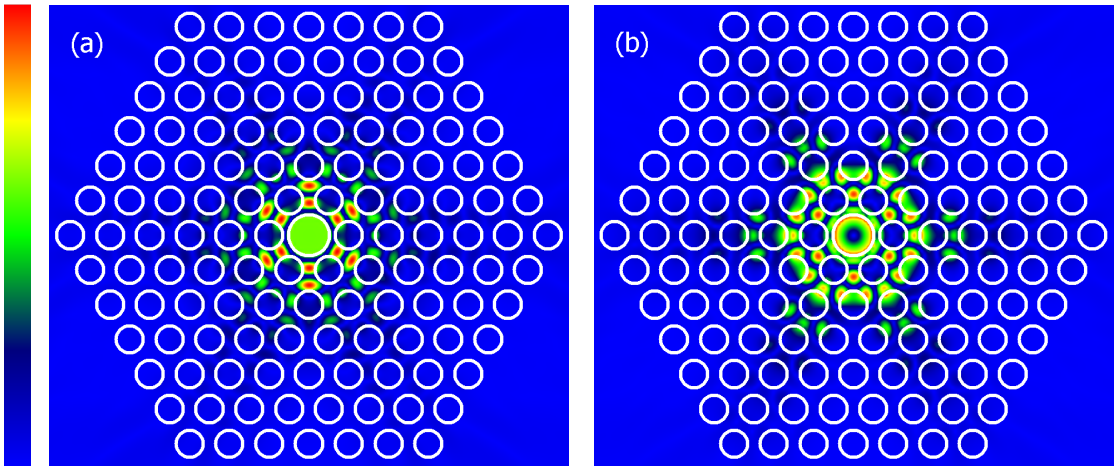

Figure 3: (a) Longitudinal and (b) radial electric field intensity of the defect mode crossing the light line in the PBG fiber as calculated with the multipole method. The white circles indicate the hole boundaries. Note that a rainbow color scheme (the legend) is used to represent magnitude with the red and blue colors being the maximum and minimum, respectively. This color scheme will be used throughout the paper for color plots from the multipole code.

with phase velocity equal to c. The longitudinal field is radially uniform within the defect. This uniformity is a direct result of the SOL condition ($v_p/c = k_0/k_z = 1$) since the Maxwell equation for the longitudinal field reduces to $\nabla_\perp^2 E_z = (k_0^2 - k_z^2)E_z = 0$, implying $E_z(r)$ = constant for the azimuthally symmetric solution ($m = 0$). The mode is like a TM_{01} circular waveguide mode. Strictly speaking this applies to an azimuthally symmetric geometry (which the hollow core approximates), but for the hexagonal geometry this results in the condition that in the lattice $dE_z/d\theta = 0$ at intervals of $\pi/6$ for the TM mode [15]. This field behavior is evident in the regions outside the defect in Fig. 3. A consequence of E_z being radially constant is that both E_r and H_θ are proportional to r in the central vacuum region for the TM mode because $E_z \sim k_z^{-1}\nabla_\perp E_\perp$. The impedance Z_c scales approximately like $(kR)^{-4}$ since the power P in the denominator is proportional to the integral of $\int E \times H r dr$. For a metallic pillbox cavity where fields terminate at the boundary, this scaling relation is very good. For a PBG dielectric fiber, the scaling is only approximate since much field energy is outside the defect, and this leads to an exponent of between 3 and 4 for geometries we have studied. Due to this strong dependence, the value of Z_c for a TM mode is mainly determined by kR when the mode is centered in the gap. Other geometry changes lead to second order improvements.

Regions of high electric field exist both at the defect boundary and outside the defect as seen in Fig. 3, and this can lead to electrical breakdown damage in the glass. The so-called damage factor ratio $DF = E_{max}/G$ of the accelerator is simply the ratio of the maximum field in the glass, E_{max}, to the accelerating field G. It determines the maximum achievable unloaded gradient in the structure when E_{max} reaches the damage threshold of the material. Because of the complicated arrangement of air holes and dielectric, enhanced electric fields can occur at so-called hotspots in the matrix, both in the transverse and longitudinal components. Certain hole sizes and locations

can be engineered to reduce these fields and displace the hotspots partially from dielectric into air holes, as we discuss in section 4. In spite of the details, an approximate scaling of DF with defect radius is empirically found in the TM fibers we have studied, specifically the ratio E_{max}/G is roughly proportional to kR. A physical explanation for this scaling is that the transverse fields increase linearly as $E_\perp \sim kRG$ in the central defect until they contact the first dielectric surface, after which they oscillate, and then decrease beyond the first layer of holes. In the matrix the oscillating transverse and longitudinal fields are of similar magnitude and regardless of which component is actually larger, the ratio is $E_{max}/G \sim kR$. Smaller values of kR are preferred for better gradient, although a compromise with particle beam aperture has to be made in an operating accelerator. For the Lin TM mode, the maximum field is in the radial direction and occurs with nearly equal magnitude at both the defect edge and in the hot-spots in the first layer of holes, giving $G/E_{max} = 0.48$ or $DF \approx 2.1$. For a laser pulse length of 1 ps operating at $\lambda = 1\mu$m, $E_{max} \approx 2$ GV/m for silica glass. Hence, the maximum gradient in the example is $G_0 \approx 1$ GV/m, a full order of magnitude higher than metallic rf structures.

2.2 Dispersion and Confinement

We generate a dispersion relation, or frequency of the defect mode as a function of the propagation constant (wavenumber), by repeating the multipole simulation for different input frequencies. The dispersion curve is shown in Fig. 4, from which the frequency of the synchronous mode propagating at the speed of light is found to be $8.15c/a$, approximately the same as that obtained in Ref. [4]. The longitudinal field distribution changes rapidly with mode wavenumber and hence phase velocity. At longer wavelengths ($k_z a$ = 6.9) the mode actually exits the band gap, becoming unconfined, and the field in the core is highly peaked. With less field energy in the matrix, the mode index is less than one and phase velocity is greater than c ($v_p = 1.08c$). At short wavelengths ($k_z a$= 9.8), the mode is still in the band gap, but the core field weakens and more field energy is in the glass, increasing the mode index above one. Even though the phase velocity is less than c ($v_p = 0.93c$), the mode becomes useless for sub-relativistic particle acceleration due to the vanishing longitudinal field.

It is instructive to see how the defect mode is confined by studying the falloff of its Poynting flux ($E \times H$) as we move outward from the defect hole. Fig. 5 shows the intensity of the longitudinal and radial components of the Poynting flux of the defect mode. The fiber region is the same as in Fig. 3, but the hole boundaries are not explicitly shown to clearly display the flux distribution. The flux is concentrated in the glass surface regions of the first two hole-layers surrounding the defect, and historically this led to the nomenclature surface defect mode being applied to any mode exhibiting this Poynting flux pattern. The Poynting flux extends to the outer boundary of holes, and results in power leaking out of the structure, accounting for the diffractive decay of this mode in a real fiber with a finite number of layers. As more layers of holes are added, the confinement improves and less radial Poynting flux escapes the fiber. The flux exhibits the hexagonal symmetry of the lattice, and this gives a clue as to the preferred directions to couple laser light into the structure and maximize energy transfer to the core. Power coupling to the fiber is not discussed in this paper, although we and our colleagues have begun work on this topic [11].

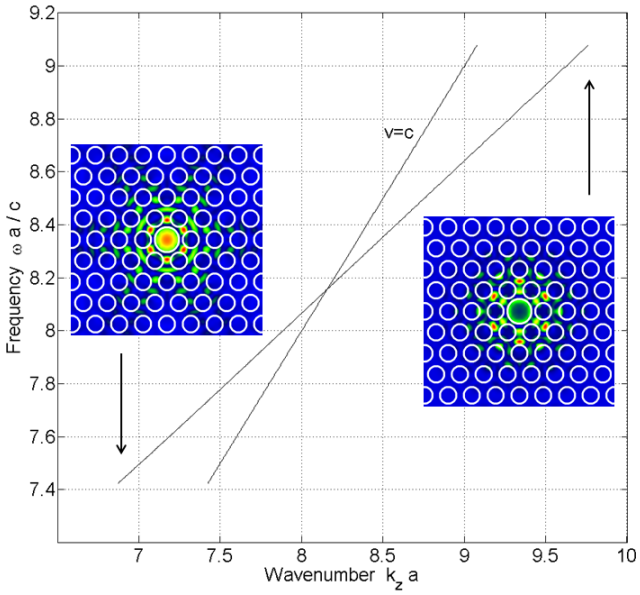

Figure 4: The TM mode dispersion curve near the light-line ($v = c$) as calculated with the multipole method. Insets show E_z field for modes at long wavelength ($k_z a = 6.9$) where $v_p = 1.08c$, and short wavelengths ($k_z a = 9.8$) where $v_p = 0.93c$.

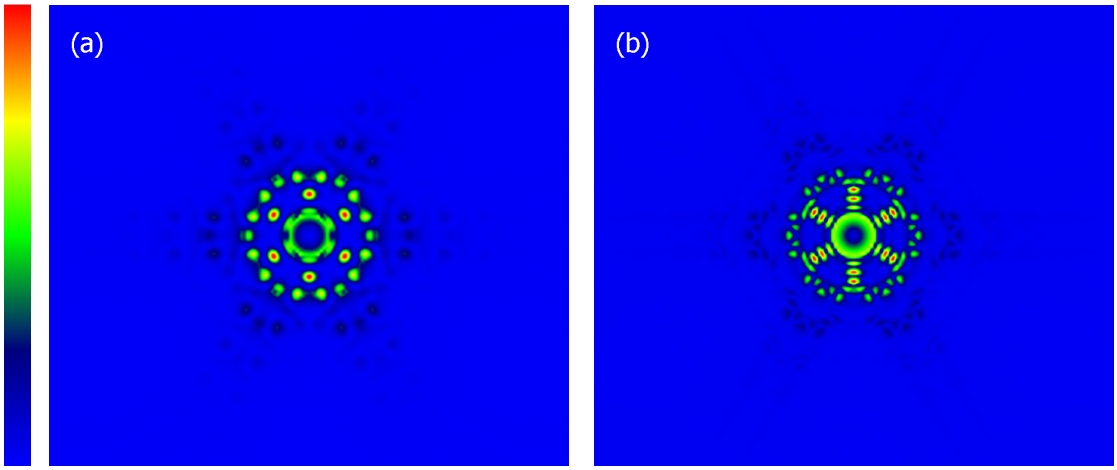

Figure 5: (a) Longitudinal and (b) radial Poynting flux of the TM defect mode in the PBG fiber. The fiber region is the same as in Fig. 3, but the hole boundaries are excluded to clearly show the extended flux distribution.

The defect modes in hollow-core PBG fibers have become recognized as belonging to two classes: core modes with Poynting flux almost entirely contained within the central hole and surface modes which are localized at the boundary separating the defect and matrix [21, 22]. Core defect modes in hollow-core fibers exhibit properties similar to TM, TE and TEM-like eigenmodes of circular waveguides, since most of their field energy is within the circular defect region, which mimics a finite, copper cavity structure. An optical communication mode is an example of a TEM core defect mode which has a transversely polarized, dipole-like field pattern, and its Poynting flux is almost entirely within the central hole. This leads to its very low attenuation with distance as needed for long-distance communication. Core modes are distinguished by the fact that their dispersion relation never crosses the speed of light line. Their effective index, $n_{eff} = ck_z/\omega$ is always less than one, and the phase velocity $v_p = c/n_{eff}$ is greater than the speed of light. The physical reason for this is the predominance of field energy in the air-core and limited overlap of the mode fields with the surrounding high index material, which keeps the effective index from being raised above one. Of course the group velocity $d\omega/dk_z$ is always less than c so although the phase velocity is superluminal, no information is transmitted faster than the speed of light.

Core defect modes are the dielectric analogs of eigenmodes in a conducting waveguide. The number of core modes $N_c(\omega)$ in a gap follows a simple analytic formula obtained by Digonnet [23], which can be written in the simplified form $N_c(\omega) \approx (Ka)^2(R/a)^2\Delta k/K$, where K is the average value of k_z in the gap region above the light-line at frequency ω, Δk is the gap width in k_z above the light-line, R is the defect radius, and a is the lattice period. Notably, this gives the estimate $N_c \approx 0.4$ for the Lin band gap due to R/a being small, and consistent with this, no core modes are found in our simulations. For accelerators one should ideally design the fiber such that $N_c < 1$ to insure no competing core modes. There are other competing modes at the same frequency as the accelerating mode but outside the band gap which are not included in this estimate. These are the so-called lattice or cladding modes which have fields throughout the matrix and often overlap with the defect as well. These modes are especially problematic since they may be excited by our drive laser and not decay away in the millimeter length of fiber. The challenge for input coupler design is to only select the desired TM mode and not launch these competing cladding modes.

Unlike a core mode, the dispersion relation of a surface defect mode can cross the light line, exhibiting an effective index that can be greater than, equal to, or less than one. The TM accelerating mode is an example of a surface defect mode [24]. The fields and Poynting flux tend to be concentrated in the matrix surrounding the defect. There is a large overlap of the fields with both lattice air holes and glass, which can result in the phase velocity being shifted significantly above or below the speed of light. Surface modes generally occur whenever a periodic lattice is terminated at a boundary [25, 26]. They are in fact lattice modes of the perfect structure with frequencies that have been sufficiently perturbed by the defect to lie in the band gap [27, 28]. The amount of glass around the defect tunes the mode frequency. Increasing the amount of glass around the core, for example by decreasing the defect size, couples the defect mode more strongly into the lower valence band and lowers its frequency. A larger defect has the opposite effect, and with less glass being present, the mode moves higher in the band gap.

Within the hollow defect region, surface modes do exhibit properties of TM, TE, and TEM modes, but outside the defect their spatial pattern does not conform to that simple behavior, being

greatly affected by the matrix structure. The distributed fields lead to diffractive loss in any real fiber with a finite number of layers. Fig. 6 shows the real and imaginary parts of the accelerating mode's effective index versus free-space wavelength for the Lin geometry, using a 6-layer multipole model and scaled to a 1.3 micron lattice period. Over this limited frequency range we use a constant material permittivity ($\epsilon_r = 2.13$) for the silica. The imaginary part of the effective index represents only the diffractive loss due to Poynting flux escaping at the matrix edge and is very sensitive to the number of layers, being about 2×10^{-4} for six layers. Confinement improves with each added layer of holes, and the imaginary part of n_{eff} decreases by about a factor of 2.5 for each layer added to the Lin fiber. But every mode decays differently according to its Poynting flux distribution. The loss coefficient $\alpha = 2k_z Im(n_{eff})$ determines the decay of the longitudinal Poynting flux with distance traveled, $S_z = S_0 \exp(-\alpha z)$. Fields are proportional to the square root of the Poynting flux, so for example, if we require the accelerating field of the Lin mode to decrease by no more than one percent over one millimeter, then the fiber must have at least 12 layers (rounded up) corresponding to $Im(n_{eff}) = 8 \times 10^{-7}$.

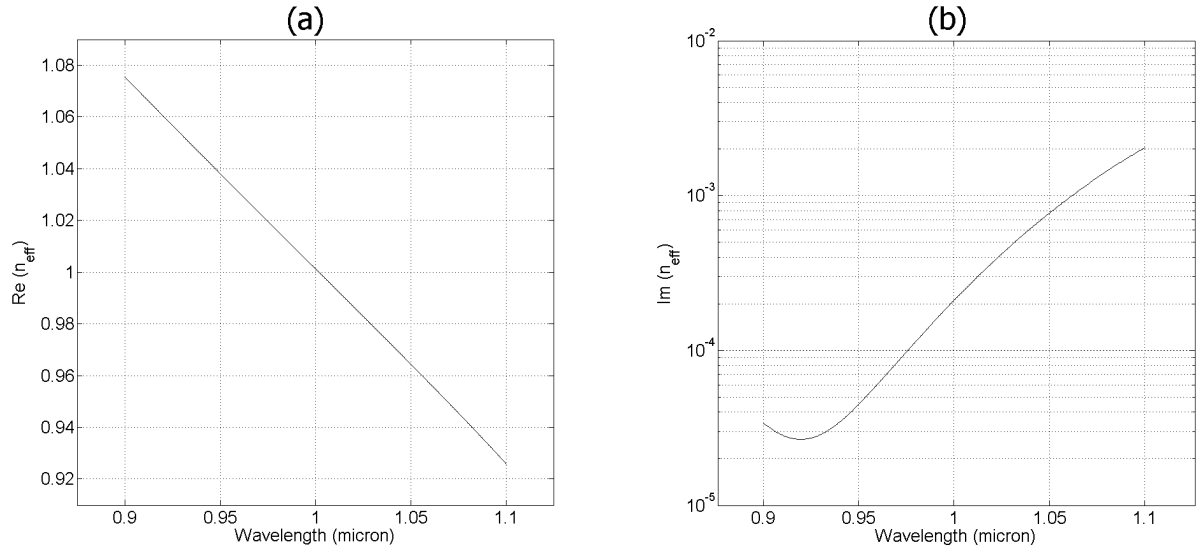

Figure 6: (a) Real part and (b) imaginary part of the defect mode's effective refractive index as a function of free-space wavelength for a six-layer PBG fiber ($a = 1.3$ micron) as calculated with the multipole method.

Fig. 7 shows the phase velocity, group velocity, and dispersion parameter for this mode as calculated with the multipole method, using a constant material permittivity ($\epsilon_r = 2.13$). One of the important features of photonic crystal fibers is the powerful control that their geometry exerts over the dispersion characteristics of modes compared to what can be accomplished with normal bulk dielectric. The dispersion parameter $D = -(\omega/\lambda)d(1/v_g)/d\omega = -(\lambda/c)d^2 n_{eff}/d\lambda^2$ measures the arrival time difference per unit bandwidth per unit distance traveled (in psec/nm/km), relative to the central reference wavelength, and essentially gives the longitudinal spread of a wave packet relative to its central value. The group velocity exhibits an extremal value when $D = 0$ since wave packet components on either side of the reference wavelength must have the same

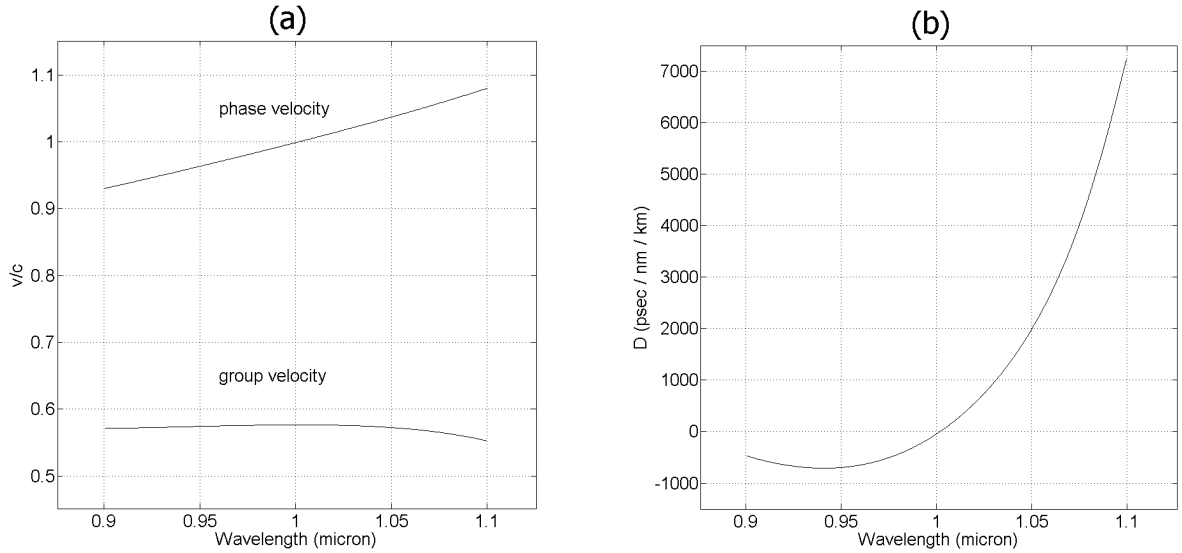

Figure 7: (a) Phase velocity, group velocity, and (b) dispersion parameter of the TM defect mode as a function of free-space wavelength for Lin PBG fiber ($a = 1.3$ micron) as calculated with the multipole method.

group velocity if the packet is not to spread. It is a useful property of the Lin mode that the group velocity is maximal and $D \approx 0$ near the light line (see Fig. 7). For a long accelerator this soliton-like behavior will keep the wave packet from spreading during the time it overlaps with the particle beam, maintaining a constant accelerating field. For millimeter long fibers, the spreading does not accumulate as much so D does not have to be strictly zero. One might also use compressive D values to advantage and maintain field strengths as Poynting flux diffracts away. Phase slip and pulse length adjustment of the same pulse is possible then as opposed to using a new shifted laser pulse for each accelerator section.

2.3 Matrix Errors

Finally we mention that wave synchronism with the particle beam will be broken if the mode phase velocity changes along the accelerator length. This will occur if the mode effective index n_{eff} changes due to randomness in lattice hole size and position as well as defect size variation. We assume that the structure is driven at a fixed laser frequency. If the structure geometry changes, then the mode dispersion line shifts, and it will be excited at a different wavenumber, shifting its phase velocity away from the speed of light, c. The change in phase velocity $v_p/c = 1/n_{eff}$ is related to the change in n_{eff} according to $dv_p/v_p = -dn_{eff}/n_{eff}$. We note that in the 1 mm prototype Incom wafers we have received, the lattice geometry with any randomness is nearly constant over the wafer length because the smooth draw process suppresses any short-scale variations in the glass. For an accelerator, we expect phase velocity changes to occur after a centimeter ($\sim 10000\lambda$) or more (without active adjustments) when we change to a different set of cut wafers.

We have used the multipole method to study the shift in n_{eff} due to changes in the defect size as well as random lattice variations. Near the light line ($n_{eff} = 1$), we find that $dn_{eff}/d(R/R_0) = -0.13$, where R/R_0 is the defect radius normalized to its design value R_0, and the variation has a sign corresponding to the change moving the mode frequency up or down. This number means that for a one percent change in defect radius R, the mode effective index changes by 1.3×10^{-3} when driven at the same laser frequency. The holes surrounding the central hole are mechanically well coupled by the large surface area of the defect. Rather than random variations, these holes tend to move together during the draw process, and the effective index variations due to changes in the first layer are $dn_{eff}/d(r/r_0) = -0.12$ and $dn_{eff}/dpos = 0.05$, where r/r_0 is the hole radius relative to its design value r_0, and pos denotes the position of the hole in the lattice normalized to its design value. If the first layer is then considered fixed to the central defect, we find that random variations of all other lattice holes give on average $\mid dn_{eff}/d(r/r_0) \mid = 0.08$ and $\mid dn_{eff}/dpos \mid = 0.08$. The individual contributions to δn_{eff} from randomness in each layer decreases as we move outward, and most of the effect on n_{eff} is from randomness in the second layer. Any hole randomness at the percent level beyond the seventh layer yields insignificant changes to n_{eff} from our simulations, presumably due to the exponentially small fields of the confined mode.

The dispersion relation of a fully synchronous, TM accelerating mode for a relativistic acceleration must cross the SOL line, and consequently it must be a surface mode. The recognition of synchronous accelerating modes as surface defect modes implies that the details of the boundary separating the defect from the surrounding matrix are the critical ingredients which determine the accelerator mode properties. As a consequence, the designs of PBG fibers for telecom applications and particle acceleration actually have opposite goals. Telecom fibers are ideally designed with no surface modes (or a limited number) since these have higher diffractive losses, and by mixing with core modes due to perturbations, they can degrade the fibers performance. A particle accelerator fiber is optimized to support a particular surface mode, and core modes are deleterious in that they may absorb input power near the operating frequency. One does not expect industrially produced telecom fibers to normally support any useful accelerating modes, so we have had to design our fibers specifically for this new purpose. This has been the focus of our collaboration with Incom Inc., and the simulation analysis of prototype TM fibers is discussed in the next section.

3 Analysis of Prototype Photonic TM Structures

3.1 Custom Defect Fibers

To realize 2-D PBG accelerating structures, the prototyping of TM mode fibers down to 1-10 microns was begun between SLAC and Incom Inc. [18], a maker of micron-scale capillary arrays, light guides, and fiber optical faceplate products used in medical and scientific applications. The prototypes are made from borosilicate glass in an industrial draw station to dimensions provided by our numerical simulations. The goals are to perfect the draw process, demonstrate dimensional control, and thereby produce a fiber accelerator that approaches gradients near the dielectric breakdown limit. These fibers serve as scaled-up models for our electromagnetic simulations using the

multipole method and BandSolve, and we assume the cross sections can be scaled down faithfully. Recall that the lattice period a is the only dimensional quantity which sets the wavelength scale, and the dimensionless ratios R/a, r/a, and the material permittivity then determine the band gap and mode properties. Actual laser accelerator sections will be realized using pure SiO2 drawn down to the final dimensions of 1-2 micron lattice periods. In this section we focus on the simulation of as-built geometries produced by Incom and the physics results we obtained. A detailed exposition of the engineering, fabrication, and beam testing will be the subject of a future joint publication.

The Incom fibers are made using an established stack-and-draw technique starting with centimeter size, glass tube stock which is heated and pulled down to micron dimensions. The larger hollow core was obtained by substituting specially sized tubes in the central region. Figure 8 shows an example of a fiber drawn down to a lattice period of about 11 microns. The central defect at this stage of the draw was approximately 12 microns in diameter. The large hexagonal unit on the left panel of the figure is about 60 lattice periods across, or about 0.7 mm. Fiber samples are sliced from meter-long strands and then polished to about 1 mm thick wafers, making up our accelerator sections. Some polishing compound remains in two lattice holes in the lower right detail of Fig. 8 prior to final rinsing of this sample.

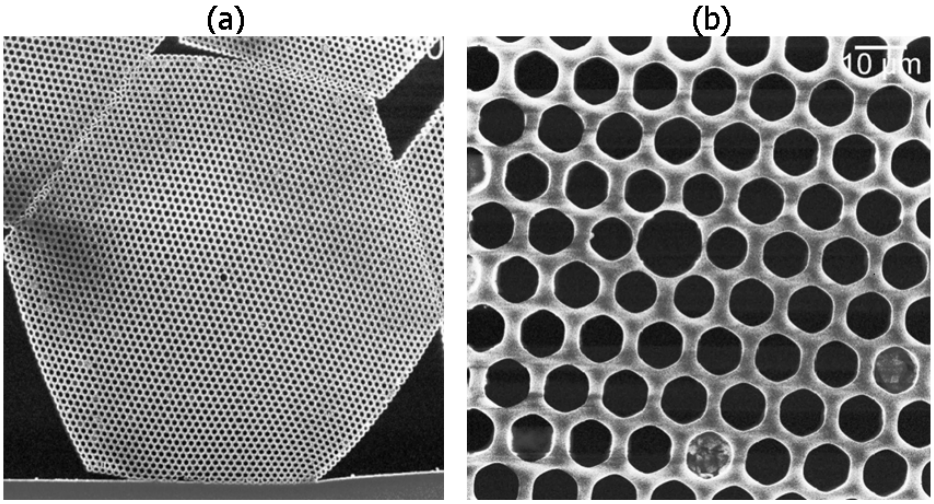

Figure 8: Photographs showing (a) 700 micron-wide cross-section of an Incom Inc. capillary fiber drawn from borosilicate glass, and (b) detail of the 12-micron central defect (Source: Incom Inc.).

The prototypes were intended to be the first fibers with dimensions specifically designed to support TM SOL modes as well as to demonstrate how to increase the accelerating field strength relative to the maximum field in the glass, where damage will occur at the highest fields. Our early simulations [24] indicated that modifying the first layer of holes could change the field strengths and distributions. For these prototypes, the defect and surrounding capillaries were sized to insure a smooth match to the surrounding lattice. Basically the central region of capillaries becomes a complicated defect which we can tune to improve our acceleration mode.

3.2 Successful Prototypes

The first prototypes were sampled at defect diameters from 12 microns down to less than 3 microns as the draw progressed. The manufacturer varied the process controls during the draws to determine their effect on hole dimensions. Sometimes the lattice and defect tended to close prematurely as the fiber was pulled. During the draw, the round tubes may take on a slightly polygonal shape as the glass flows. This is seen in Fig. 8. But owing to the large volume of glass to air, we find that computationally the slightly hexagonal holes can be approximated as round holes in BandSolve with no change in the calculated band gap. The round-hole approximation is a major simplification and is used in both our multipole and BandSolve calculations. This is different from the simulations of the honeycomb telecom fibers to be discussed in Section 5 where the hexagonal holes bordered by thin glass walls must be correctly modeled in BandSolve owing to the glass to air ratio being less than ten percent.

Dimensions and positions of the holes and defect were measured by the manufacturer from photo-micrographs of the fibers. These fibers had about 1 percent variation in the lattice period and 2-4 percent variation in hole size across the transverse sample, small enough to not modify the band gap. For a scaled model we need the ratios of the hole sizes relative to the lattice period to use in our electromagnetic calculations since we assume that the ultimate silica fibers will be drawn down to 1-2 micron periods. We use the relative permittivity $\epsilon_r = 2.13$ in all our calculations, appropriate for silica at wavelengths of 1-2 microns.

Of the several samples made by Incom in the first experimental draws, two fibers have parameters suitable for TM modes. We present numerical analyses of these two fibers which have lattice periods of 9.8 and 4.9 microns, respectively. The 9.8 micron fiber has matrix parameters $r/a = 0.363$ and $R/a = 0.463$. Its defect was slightly smaller than desired and demonstrated how the TM mode can be detuned to lie at the bottom of the band gap, as illustrated by Figures 9, calculated with BandSolve. The 4.9 micron fiber has parameters $r/a = 0.33$ and $R/a = 0.53$, which are remarkably close to the theoretical Lin model. From our numerical analysis, this fiber has dimensions to support a TM SOL mode properly tuned to the band gap, the first such prototype realized to our knowledge. This fiber only needs to be scaled down about a factor of two to achieve the accelerator structures we desire for the particle acceleration experiments, a demagnification factor that should be achievable with the Incom draw process. We remind the reader that silica is transparent below 2.1 micron wavelength and exhibits various absorption bands at longer wavelengths [5]. These scaled-up prototype fibers with periods greater than about 3 microns will not transmit accelerating modes over long distances, but limited transmission will probably occur over a millimeter sufficient for an experimental measurement.

We discuss the 9.8 micron-period fiber first. The ratio r/a for the lattice holes was 0.363 at this stage of the draw. The dimensions were intended to be near a so-called Incom-D design that was achievable for the tube stock available at the time. This fiber attempted an improvement in gradient divided by maximum field in the glass, compared to the Lin conceptual design [4]. The holes of the first layer around the defect have radii $r_1/a = 0.33$, slightly smaller than the lattice holes. The central defect was intended to have $R/a \geq 0.52$, but it tended to close during this stage of the

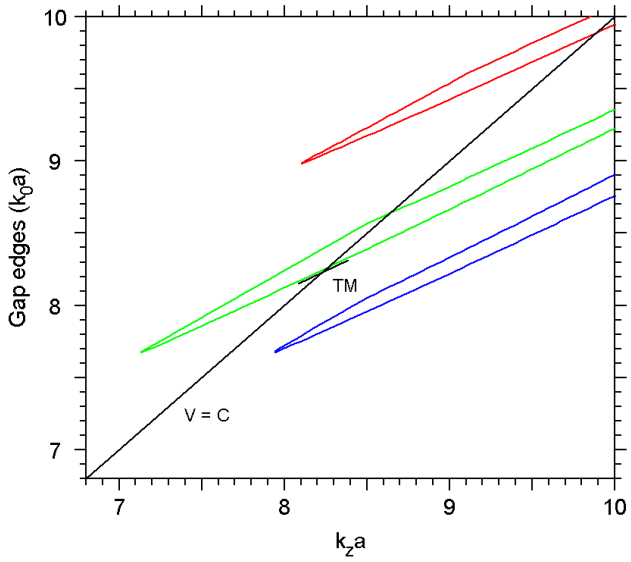

Figure 9: Band gap diagram of the 9.8-micron period fiber (defect R/a = 0.463, lattice hole r/a = 0.363) fabricated by Incom Inc. showing location of TM accelerating mode as calculated with BandSolve.

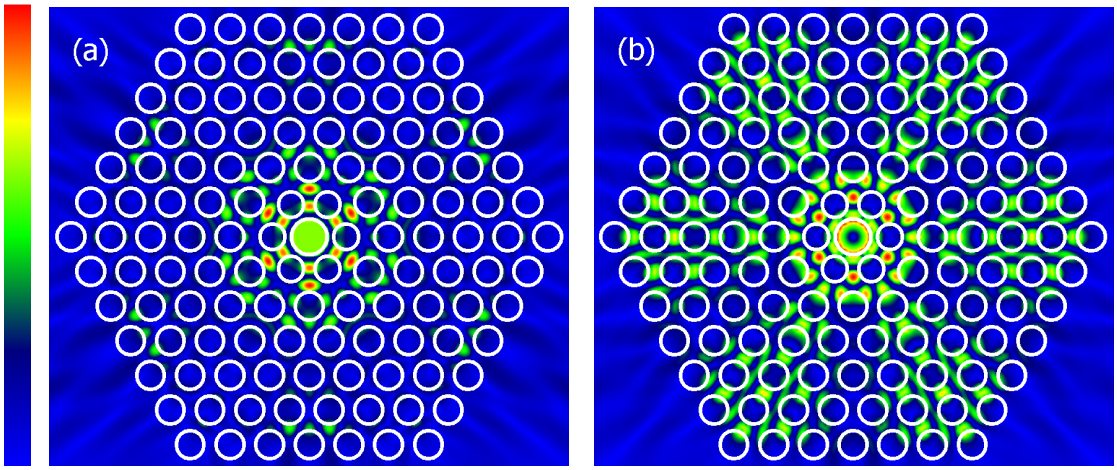

Figure 10: (a) Longitudinal and (b) radial electric field intensities calculated with the multipole method for the TM defect mode of the 9.8-micron fiber.

draw, resulting in a ratio 0.463, about 11 percent less than desired. Figure 9 shows the band gap for this lattice as calculated with BandSolve. The smaller defect means that the TM defect mode frequency is lowered, crossing the light line at about $k_z a$ = 8.2. This phenomenon was discussed in Section 2 as being a natural detuning that occurs for surface modes when the increased amount of glass couples the mode more strongly into the lower valence band.

In spite of this detuning, the TM mode is still identifiable in our simulations as a partially confined mode, as shown in Fig. 10. The gradient is $G/E_{max} = 0.54$ for this mode compared to 0.48 for the Lin design. The plot of the radial electric field gives physical insight into why this ratio is improved. The highest fields are in the radial direction with a maximum at the six hot-spots in the first layer of holes (radial position $1.1a$). Longitudinal fields remain well confined, but radial fields are more distributed and weakened compared to the Lin mode. This reduces the radial fields at both the defect edge and in the lattice while the longitudinal field is maintained. Unfortunately with the mode at the bottom of the band gap, the Poynting flux is less localized around the defect, and the higher integrated power results in the impedance ($\sim G^2/P$) being reduced to about 8 ohms compared to 19 ohms for the Lin mode. This suggests a possible trade-off in impedance and maximum field value, but further prototyping is needed to clarify this.

The 4.9 micron-period fiber was similarly modeled numerically, and a properly confined TM mode was identified in our simulations. This fiber has matrix parameters $r/a = 0.33$ and $R/a = 0.53$, while the holes of the first layer around the defect have radii $r_1/a = 0.3$, again giving us some control of modal properties. Fig. 11 shows the band gap diagram of the 4.9 micron fiber calculated with BandSolve, assuming a permittivity of 2.13. A portion of the dispersion line for the TM mode crossing the light line at $k_z a$ = 7.9 is shown. It is clearly localized in the gap, demonstrating that the manufacturer can control dimensions at the micron-scale adequately to tune the accelerating mode. This mode is found in both the multipole and BandSolve calculations, and it has a field ratio of $G/E_{max} = 0.48$, an impedance of 19 ohms, and a group velocity of $0.57c$.

The longitudinal and radial electric fields of this TM mode are plotted in Fig. 12, and a line-out plot of the longitudinal field along the two transverse dimensions is shown in Fig. 13 when scaled to the same 1.3 micron lattice period as the Lin example discussed in section 2. The longitudinal field is uniform in the defect as desired for a TM SOL mode. The highest fields are in the radial direction and located on the defect edge, while the radial fields at the hot-spots in the first ring are reduced in this geometry compared to the Lin mode in Fig. 3. This demonstrates that the maximum fields can have their positions shifted in the matrix by defect modification, while maintaining the same impedance and ratio of G/E_{max}.

The phase velocity, group velocity, and dispersion parameter of the mode as a function of free-space wavelength $\lambda = \omega a/c$ are plotted in Figure 14 using the multipole method when scaled to the same 1.3 micron lattice period as the Lin example. The mode crosses the light line at 1.037 microns, but at this point the group velocity is not a maximum, and the dispersion parameter is about $D = -1200$ psec/nm/km. This should be compared with the behavior for the Lin mode which has $D = 0$ at the light line. We find that non-zero values of D (and non-maximal group velocity) occur at the light-line when the TM mode is not centered in the band gap. We emphasize that this example corresponds to a real, as-built fiber as opposed to an ideal fiber. In the next

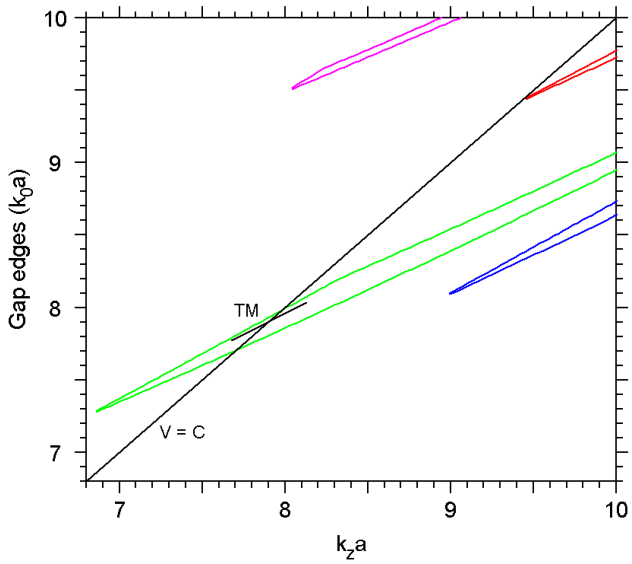

Figure 11: Band gap diagram of the 4.9-micron period fiber (defect R/a = 0.53, lattice hole r/a = 0.33) fabricated by Incom Inc. showing location of TM accelerating mode as calculated with BandSolve.

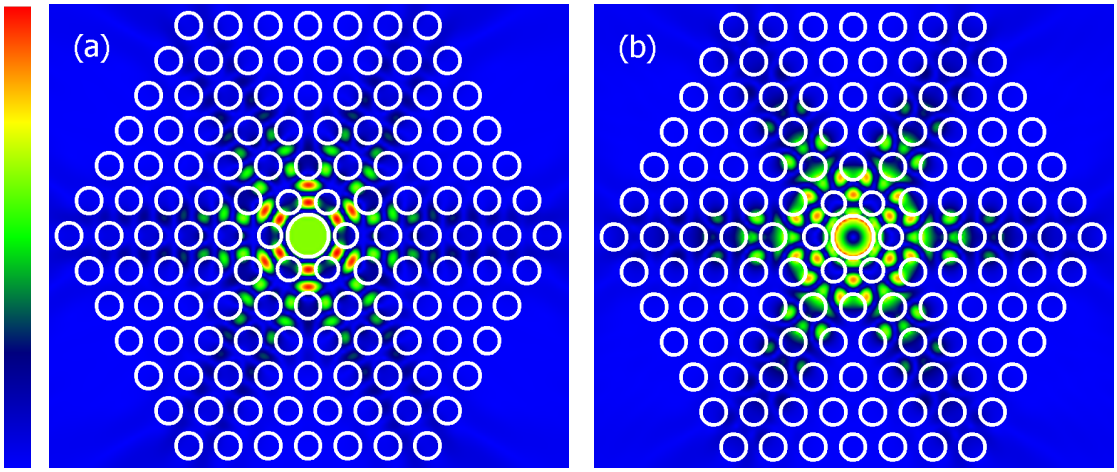

Figure 12: (a) Longitudinal and (b) radial electric field intensities calculated with the multipole method for the TM defect mode of the 4.9 micron-period fiber.

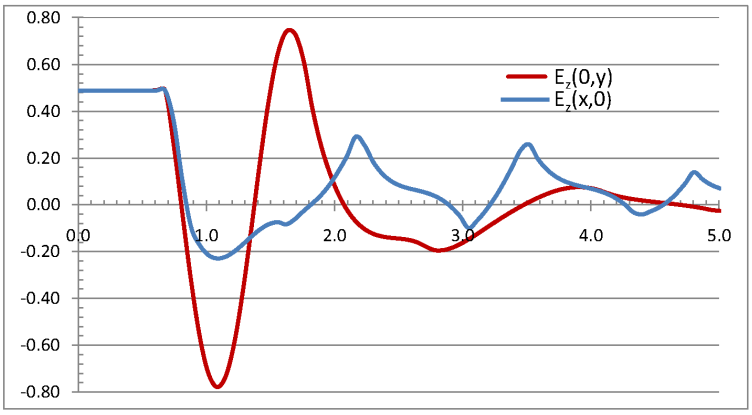

Figure 13: Line-out plot of the TM mode longitudinal field (arbitrary units) calculated with the multipole method along the two transverse dimensions (in microns) for the 4.9 micron fiber when scaled to a 1.3 micron lattice period.

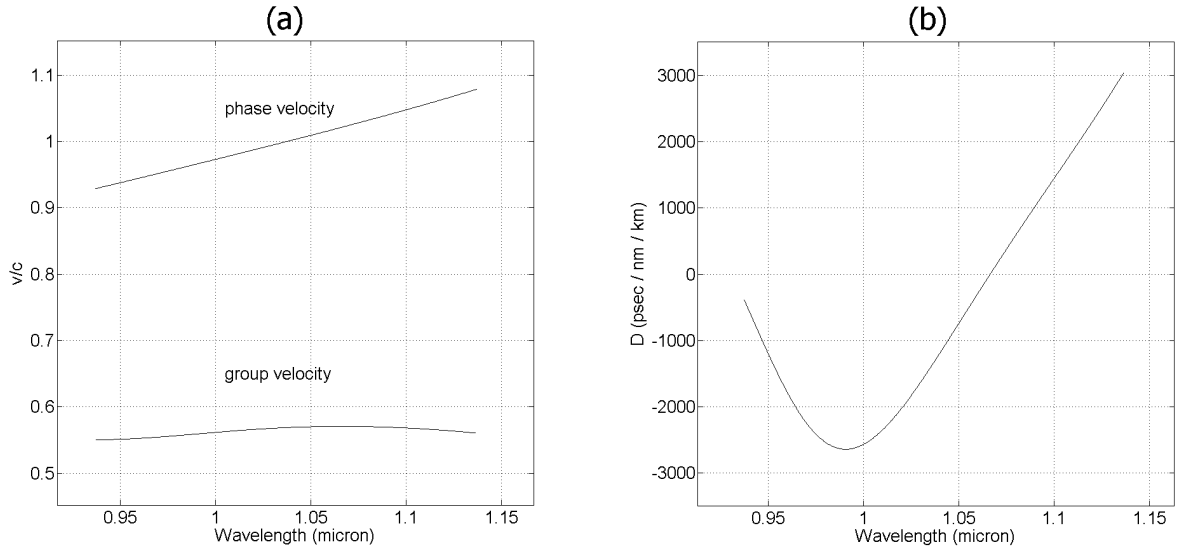

Figure 14: (a) Phase velocity, group velocity, and (b) dispersion parameter of the TM defect mode as a function of free-space wavelength for the 4.9 micron-period fiber when scaled to a 1.3 micron lattice period.

section we describe briefly some improvements to the basic geometry that one can explore to optimize future prototype fibers.

4 Matrix Modifications to Improve TM Modes

In the foregoing, we discussed our analysis of the Incom fibers and the first attempts to improve the design. During prototyping it was decided in the interest of time to use existing capillary stock to see whether an acceptable fiber accelerating mode could be made to verify our calculations. The fiber with 4.9 micron period survived the simulation tests showing a good TM mode in the gap, and this is the one we have focused on. In this sense, the first test was a remarkable success. Here we briefly discuss a few examples of design changes that we have studied numerically to improve the benchmark Lin design. There are many options still to be investigated. We explored reducing or eliminating holes, changing their permittivity, and making lattice perturbations such as aperiodic inclusions or other holey insertions. These modifications will change the distribution of fields and can potentially improve the gradient and impedance.

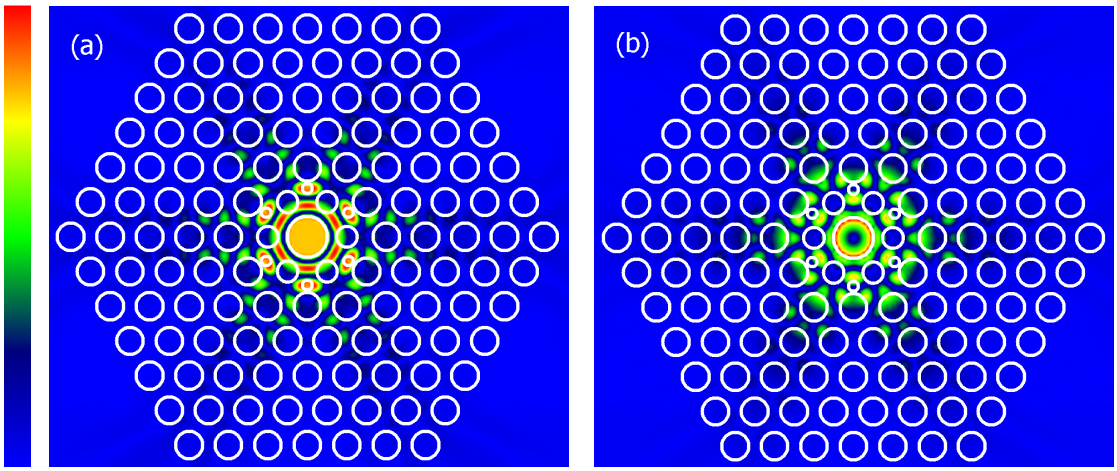

Figure 15: (a) Longitudinal and (b) radial electric field of the TM mode calculated with the multipole method for a Lin-type fiber with extra micro-holes in the defect region.

In section 2 we noted that when the TM mode is well centered in the band gap, the value of kR had the strongest effect on the impedance. Our analysis of the 4.9 micron Incom fiber indicated that the TM mode was in the band gap but not centered. The defect radius is $R/a = 0.53$ and is slightly larger than ideal, which moves the mode up in the gap. Reducing the defect radius to $R/a = 0.51$ tunes the mode to the gap center at $k_z a = 7.8$ and reduces the value of kR by about five percent. The impedance increases significantly to 24 ohms, and the gradient ratio is improved to $G/E_{max} = 0.51$ according to our simulations. With the mode centered in the gap, the dispersion parameter $D \approx 0$.

As a second example, we show in Fig. 15 a design variation intended to flatten the maximum fields in the lattice. We added six micro-holes between the first and second layers at the location

of the hot spots in the longitudinal field and reduced the hole radii of the first layer to keep the mode crossing the light-line ($n_{eff} = 1$) at about the same $k_z a$. Such micro-capillaries in the PBG lattice are the analogs of dopants in semiconductors or lasers acting as small interstitial atoms (e.g. hydrogen) to modify the crystal properties, and in this case they are at the level of five percent by capillary number. This modification resulted in the ratio of the accelerating field in the defect to the maximum longitudinal field in the glass increasing from 0.62 to 0.82. We note that the field uniformity in the defect is retained here while the pockets of strong E_z and E_r field in the lattice have become more distributed and weaker when compared to the Lin geometry in Fig. 3. The radial fields are still the highest overall but only on the defect edge, being reduced in the lattice. The ratio of G/E_{max} is 0.48, and the characteristic impedance of this mode is 15 ohms. No attempt was made to optimize any other parameters beyond improving the longitudinal field on axis relative to that in the glass.

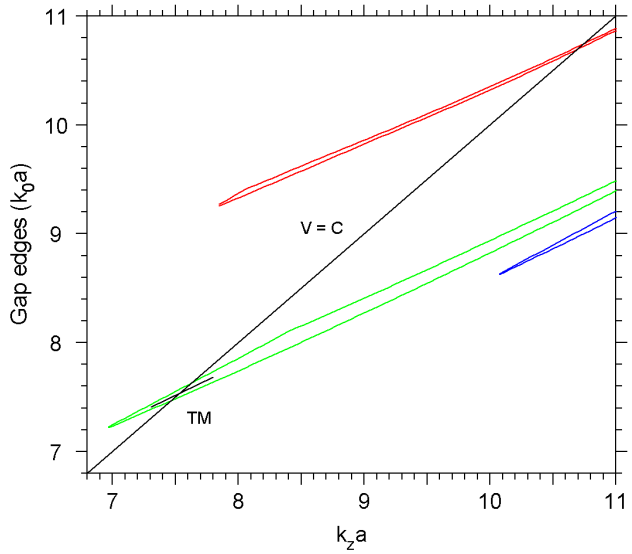

Figure 16: Band gap diagram calculated with BandSolve of a high-impedance TM mode fiber, showing the location of the SOL mode for the matrix parameters r/a = 0.31 and R/a = 0.478.

Finally we present an example of a TM fiber design with significantly higher impedance and gradient compared to the Lin example. The strong dependence of Z_c and G/E_{max} on kR means we should aim for a confined mode in a band gap which is lower in ka but still crosses the light line. We reduce the lattice hole size of the Lin geometry to $r/a = 0.31$, and the gap now crosses the light line near $ka \approx 7.5$ as shown in Fig. 16. This gap moves below the light line if the hole size is reduced further. Adjusting the defect size to $R/a = 0.478$ we find a TM mode crossing the light line at the gap center $k_z a = 7.54$, as indicated in the figure. The kR value of the mode is 14 percent less than the Lin example, and this has a major effect on the mode properties. The characteristic impedance is 28 ohms, approximately a 50 percent increase over the Lin design. The field intensities are shown in Fig. 17. The highest fields are radial and at the defect edge. The gradient ratio is $G/E_{max} = 0.55$, having increased linearly with $1/kR$. One negative attribute is that because this gap is narrower, the confinement is six times poorer than the Lin mode. We would need to add two more layers of holes in an operational fiber to recover the same $Im(n_{eff})$.

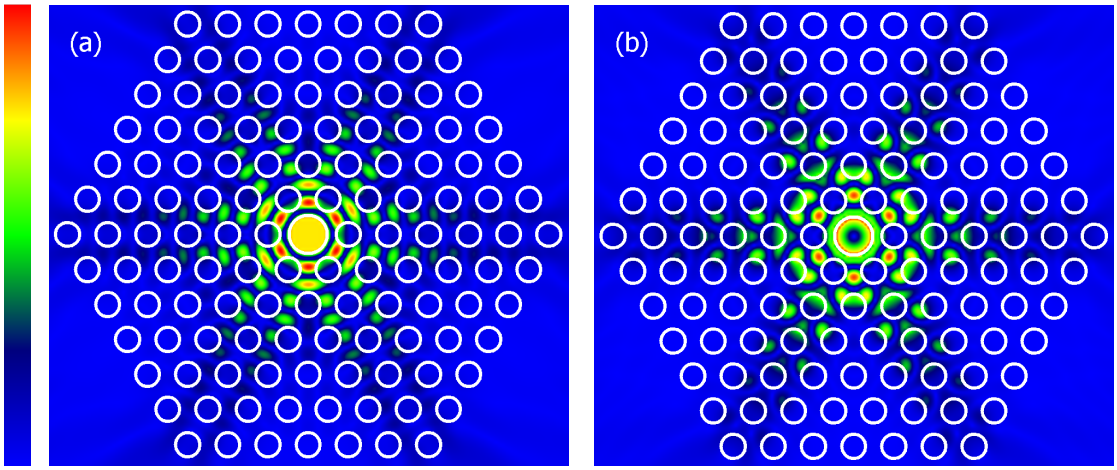

Figure 17: (a) Longitudinal and (b) radial electric fields of the high-impedance TM SOL mode calculated with the multipole method.

5 TM Surface Modes in Telecom Fibers

As we mentioned earlier, the designs of PBG fibers for telecommunication applications and particle acceleration have opposite goals. Telecom fibers are designed to support a TEM core mode with few or no surface modes. A particle accelerator fiber is optimized to support a particular surface mode, and core modes are deleterious in that they may absorb input power. We do not expect industrially produced telecom fibers to support any useful accelerating modes. But we can use these fibers to benchmark our codes and investigate the nature of fiber modes for laboratory experiments. Telecom fibers are not totally free of surface modes, and some of these can be TM modes.

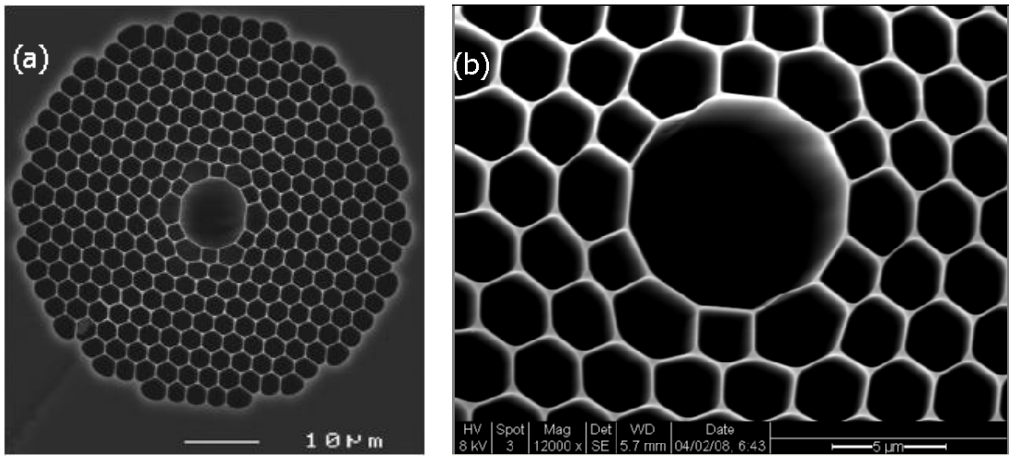

Figure 18: SEM photographs showing (a) cross section of the commercial HC-1060 telecom fiber (NKT Photonics [29]) and (b) detail of the central defect (Stanford/SLAC photo). The lattice period is 2.75 microns and the central defect diameter is about 9.5 microns.

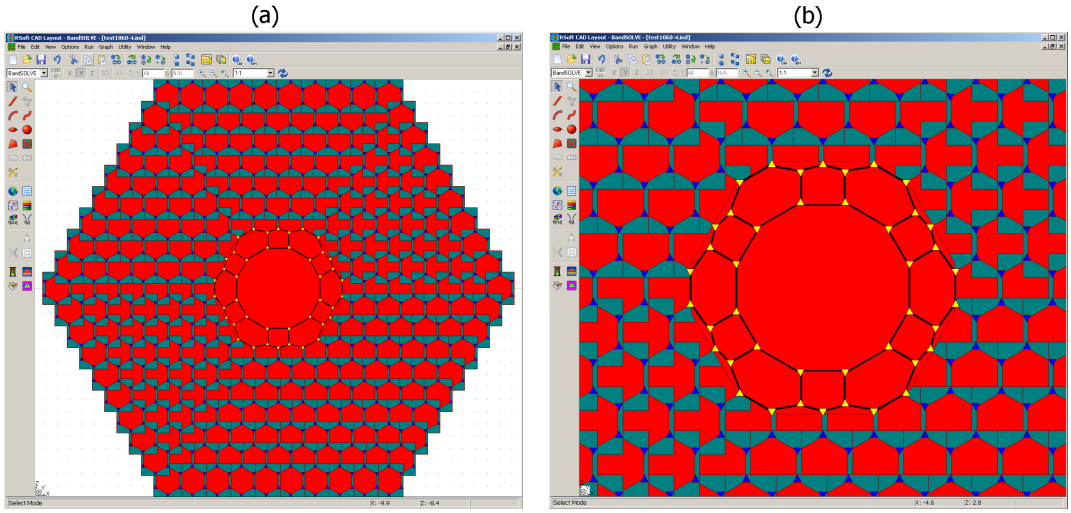

Figure 19: (a) CAD model of the HC-1060 fiber constructed in R-Soft BandSolve and (b) detail of the defect region constructed of glass walls (black, $0.036a$ thick, a = 2.75 micron) and glass triangular vertices (yellow, $0.16a$ on an equilateral side).

We have numerically modeled the HC-1060 fiber made by NKT Photonics (formerly Crystal Fibre) [29] using R-Soft BandSolve to search for any TM SOL modes which could be excited by a relativistic electron beam. The HC-1060 fiber is made of silica glass (ϵ_r = 2.13) and its cross section is shown in Figure 18. The lattice has a period of 2.75 microns in the horizontal plane, the matrix is more than 90 percent air by volume, and the hollow defect is about 9.5 microns in diameter. The defect region is very complicated and includes deformed cells in the two layers surrounding the central hole.

The R-Soft CAD model of the HC-1060 fiber is shown in Figure 19. The band gap diagram is determined by the perfect lattice without defect. The lattice was constructed by laying down a series of honeycomb cells with the hierarchal tiling tool in the R-Soft CAD program following the electron microscope photographs. The cell dimensions were fine-tuned so the calculated bandgap position and width ($\sim$110 nm) agreed with the vendor plot of attenuation versus wavelength for the telecom modes (proxy for the bandgap where confined modes exist). We find that the glass wall thickness sets the gap central value of $k_0 a = \omega a/c$. Thinner webs push the gap diagram to higher frequencies. The glass vertex size (the point where three walls meet) sets the band gap width. Larger vertices widen the band gap. The bandgap is shown in Fig. 20. To model the defect, the central portion of the lattice was then removed, and a customized defect was constructed with triangular glass vertices and glass walls (using Combine/Merge mode for overlapping segments). The wall thickness and triangular vertex size were the same in the defect as in the lattice. Supercell computation domains of 10X10, 12X12, and 14X14 lattice periods were used in BandSolve to test the faithfulness of defect mode calculations. The 12X12 supercell usually gave a consistent determination of the effective index and mode pattern. Typically larger supercells are needed for larger defects to avoid field cross-talk at the periodic boundaries of the calculation domain.

In our BandSolve simulation of the HC-1060 fiber, we found the expected telecom TEM core

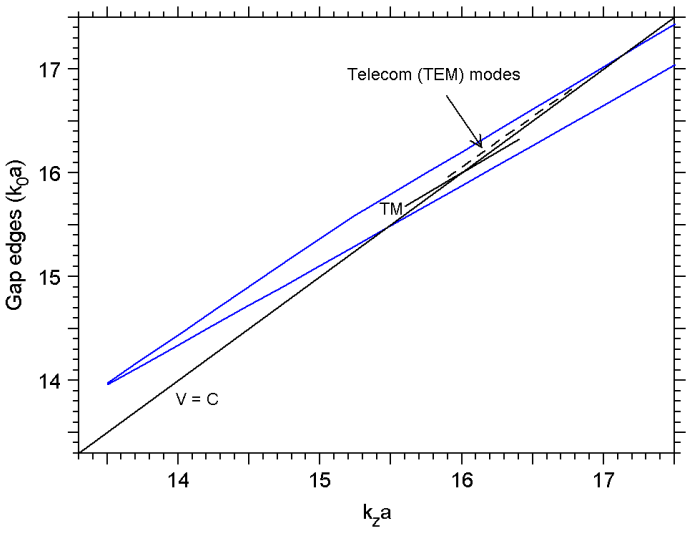

Figure 20: Band gap diagram of the HC-1060 fiber showing location of telecom modes (dashed line) and TM defect mode (solid line) relative to the light-line (v = c) as calculated with R-Soft BandSolve.

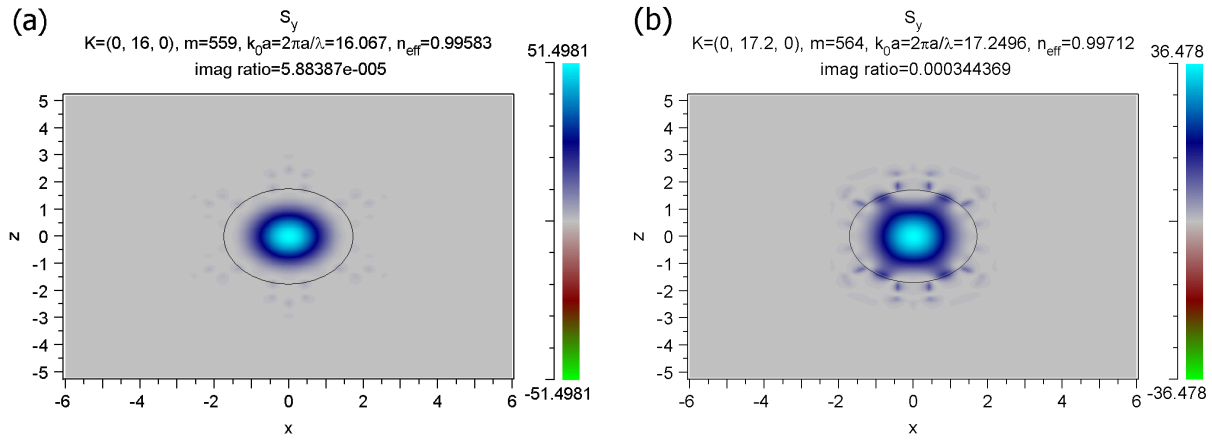

Figure 21: Longitudinal Poynting flux of the telecom mode in the HC-1060 fiber as calculated with BandSolve at (a) wavenumber $k_za = 16$ and (b) at band gap upper edge $k_za = 17.2$ where confinement is lost. The solid ellipse denotes the boundary of the central defect hole.

modes with no other adjustments to the model. There are two telecom modes, nearly degenerate in frequency, but with electric fields predominantly polarized along the two transverse directions. Being core modes, their effective index remains less than one, and their phase velocity is always greater than c (about $1.004c$ for the telecom modes). Telecom dispersion lines run along the top of the light line as shown in Fig. 20 from $k_z a$ = 15.4 to 17.1 (or λ = 1.12 to 1.01 microns) with a nearly constant group velocity of $0.93c$. Outside the bandgap these modes have significant field energy in the matrix, confinement is lost, and they diffract away in a real fiber with finite boundaries. The longitudinal Poynting flux of a telecom mode near the band gap center at λ = 1.08 microns ($k_z a$ = 16) and at the band gap upper edge ($k_z a$ = 17.2) is shown in Fig. 21. Note that the flux spreads transversely when the mode approaches the upper gap edge where confinement is lost. A similar behavior is found at the lower gap edge. In the BandSolve convention, the transverse directions are x and z, and the longitudinal direction is denoted by the y-coordinate (which we normally designate by z in accelerator applications). The metric called *imag ratio* in the plot header is a measure of how well BandSolve orthogonalized the eigenmode and separated it from nearby modes. If this metric is of order 10^{-2} or less, the mode is adequately separated, and the field intensity plot is a good representation.

In addition to the telecom modes, the BandSolve simulation yielded about a dozen other core modes and many surface modes. The number of core modes is consistent with Digonnet's formula [23], which gives $N_c \approx 15$ at the widest part of the HC-1060 band gap, mainly due to the large defect size, $R/a = 1.73$. The code found four TM-like surface modes crossing the light line, but only one mode near $k_z a = 16$ (1.08 micron) had any significant accelerating field. Its location is noted in the band gap diagram of Fig. 20. This accelerating mode is very weak and has a longitudinal field on axis divided by the maximum field in the glass of $G/E_{max} = 0.006$. The longitudinal electric field of the TM mode is shown in Fig. 22. The quadrupole pattern of the TM mode is an artifact of the rectangular boundaries. This splits the true mode into two, and a second TM-like mode (with $E_z \simeq 0$ on axis) is found nearby in frequency, also shown in the figure. When superimposed the two modes exhibit the correct hexagonal symmetry. A simulation with a larger 14×14 supercell resulted in the two modes getting closer in frequency and less coupled to the boundary, so we expect with a large enough supercell the true single mode would emerge. Cleanly separating surface modes is a major computational difficulty with large-defect fibers.

The TM SOL mode is extraordinarily inefficient for acceleration with a characteristic impedance $Z_c = 0.005\ \Omega$. The low impedance of this mode is attributable to the large defect radius relative to the wavelength. Taking the ratio of $(kR)^{-4}$ between the Lin fiber and the HC-1060 fiber, we would estimate $Z_c \approx 0.01\Omega$, within a factor of two of the simulation result. With so little glass in the fiber, the mode group velocity $v_g = 0.81$ is relatively high at the light line. The field flatness of the mode in Fig. 22(a) is $\Delta E_z/G \approx 0.25$ in the central region $r < 0.5a$, with the field tending to increase along the horizontal axis and decrease along the vertical axis. This asymmetry is partly due to the aforementioned mode splitting, and the field uniformity would improve if the two nearly degenerate modes were combined.

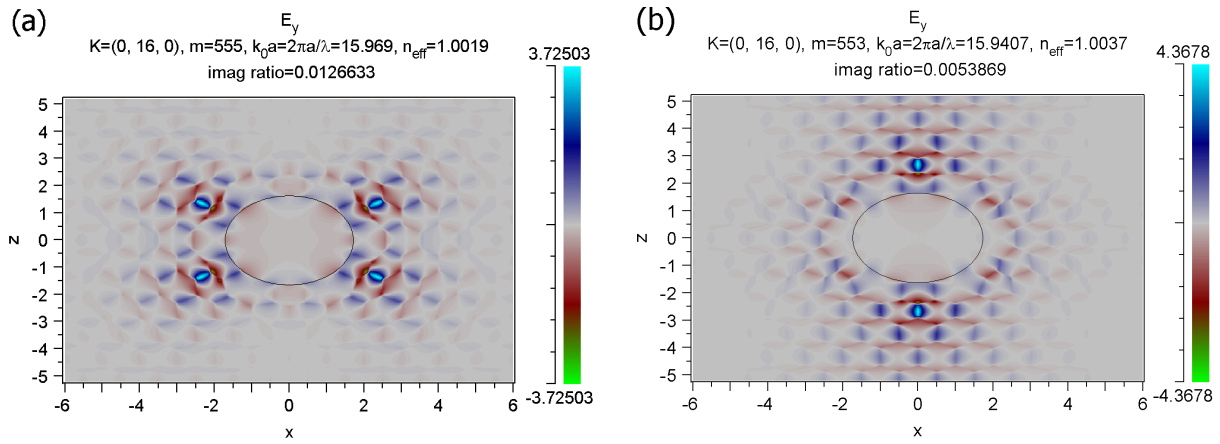

Figure 22: Longitudinal electric fields of the two nearly degenerate TM surface modes crossing the light-line for the HC-1060 fiber as calculated with BandSolve for a value of $k_z a = 16$. The solid ellipse denotes the boundary of the central defect hole.

6 Conclusion

In this paper we have focused on the basic electromagnetic properties of the accelerating modes in 2-D hollow-core PBG fibers and specifically to the geometry changes that will improve both the characteristic impedance and the ratio of acceleration gradient to maximum field. Wherever possible we provided physical insight into accelerating mode behavior based on the surface mode nature and the distinction with core defect modes. The latter mode type is almost completely localized in the hollow core with phase velocity always greater than the speed of light, and is exemplified by the TEM-like modes used for telecommunications. Surface modes are predominantly confined to the defect region but with significant field in the surrounding matrix, leading to a phase velocity that may equal the speed of light. This makes them suitable for synchronous, relativistic particle acceleration, and is the main reason why the design of telecom and accelerator fibers is so different.

We have reported on our numerical analysis of the first prototype fibers fabricated by our industrial partner which were specifically designed for speed of light TM modes. These fibers were drawn from centimeter size, glass tube stock down to a few microns with dimensional ratios and tolerances suitable for TM modes. Hollow-core fibers with a single defect in a lattice with up to thirty layers of surrounding holes were made in optically polished, millimeter-thick wafers. The prototypes are only about a factor of two larger in scale than needed for our final accelerator structures which are now being fabricated. Finally we also explored the presence of TM-like SOL modes in commercial telecom fibers which are being used in our SLAC beam experiments to generate wakefields at the TM mode frequency with relativistic beams. This will serve to calibrate our codes with experimental mode spectra.

The numerical analysis of real prototypes has improved our physical understanding of PBG accelerating modes. The tuning of the defect mode frequency to the band gap center by adjusting the defect size is now seen as necessary to maximize the characteristic impedance, maximize the group velocity, and null the dispersion parameter simultaneously. Interestingly if a non-zero

dispersion parameter and a slightly reduced impedance are acceptable, we found that when a TM mode is detuned up or down from the gap center, the transverse fields lose confinement more than the longitudinal fields, causing the ratio of G/E_{max} to improve. This may be a useful trade-off to reduce the damage factor. Overall the strongest parameter to control impedance and the ratio of gradient to maximum field in the glass is the defect size divided by wavelength, with smaller ratios being preferred. To this end, the matrix geometry should be designed with the band gap crossing the light line at a low value of ka, and kR adjusted to as small a value as possible consistent with a TM mode being in the gap center.

The prototype fibers demonstrated the level of random errors that results from a draw when no special precautions are taken to insure a steady-state flow. Randomness in matrix parameters will change the mode phase velocity and cause loss of particle synchronism. The prototypes were typically cut from meter-long sections during a transient pull from the heating fixture. Random errors of about one percent in the lattice spacing and 2-4 percent in hole sizes were obtained. These are quite good for a transient pull, but further prototyping is needed to determine the ultimate level that can be achieved in steady-state. In section 2 we quoted the expected variations in effective index and phase velocity for Lin-type fibers, and this indicates that the relative phase velocity variations are about 10^{-3} for one percent variations in the matrix parameters. Due to the exponentially small fields far from the defect, we find the phase velocity is insensitive to one-percent lattice randomness beyond the seventh layer of holes.

We have provided a reasonably complete discussion of the electromagnetic aspects of PBG fiber acceleration modes with the goal of illustrating the design requirements and techniques to realize TM fibers and ultimately bring these to full experimental test and verification. A more detailed exposition of the engineering, fabrication, and beam testing of prototype fibers will be provided in a forthcoming paper. We have limited the scope of this paper to the accelerator mode properties and excluded beam loading and input power coupling issues. Optical power coupling at the end of a Lin-type fiber has been studied [11], and a paper on the side-coupling of power to a fiber is in progress. Interaction of beams with the accelerator structure is part of the ongoing experimental program at SLAC [12] and specifically the measurement of wakefields and synchronous particle acceleration will be discussed in a future publication. Results from the experimental program will guide us in a better understanding of how these optical scale structures behave with particle beams.

The field of PBG fiber acceleration is complex with many challenging problems, but with prototype structures now available, we can envision the first beam experiments followed by structures with realistic input couplers and beam focusing elements on a timescale of perhaps five years. At each increment of energy, there should be many intriguing and practical applications to be pursued as we realize microscopic particle accelerators.

Acknowledgements

The authors thank Prof. Robert L. Byer, Eric Colby, Ben Cowan, R. Joel England, Rasmus Ischebeck, Rachik Laouar, Chris McGuinness, Cho-Kuen Ng, Johnny Ng, Edgar Peralta, Tomas

Plettner, Chris Sears, Prof. Robert H. Siemann, Ken Soong, Dieter Walz, Ziran Wu, and Di Xu for their encouragement, support, and discussions during this work. We thank Patrick Lui for his work to establish and maintain the industrial collaboration. We thank our Incom Inc. colleagues for the engineering and fabrication of prototype TM fibers and especially D.C. Bennis, C.A. Craven, M.A. Detarando, M.J. Minot, J.A. Krans, R.J. McLaughlin, J.M. Renaud, and D.W. Stowe. The work at SLAC is supported by the U.S. Dept. of Energy contract DE-AC02-76SF00515. Incom's fabrication effort was supported by DOE STTR Phase I award DE-FG02-09ER85425. SLAC supported that project under a funds-in CRADA with Incom. The work at the University of Sydney was supported by the Australian Research Council (ARC) under the Centre of Excellence and Future Fellowship Schemes.

References

[1] K. Soong et al, Experimental Determination of Damage Threshold Characteristics of IR Compatible Optical Materials, in Proceedings of 2011 Particle Accelerator Conference, (IEEE, New York, NY, 2011), paper MOP095.

[2] M. Rosing and W. Gai, Phys. Rev. D**42**, 1829 (1990).

[3] A. Mizrahi and L. Schachter, Phys. Rev. E**70**, 016505 (2004).

[4] X. E. Lin, Phys. Rev. ST Accel. Beams **4**, 051301 (2001).

[5] Newport online catalog, Optical Materials section, [http://www.newport.com/store/genContent.aspx/Optical-Materials/144943/1033].

[6] S. John, Phys. Rev. Lett. **58**, 2486 (1987).

[7] E. Yablonovitch, Phys. Rev. Lett. **58**, 2059 (1987).

[8] R.F. Cregan et al, Science **285**, 1537 (1999).

[9] B.J. Mangan, in Optical Fiber Communications Conf. (Opt. Soc. Amer. 2004), paper PDP24.

[10] N. Kroll, D. R. Smith and S. Schultz, in Advanced Accelerator Concepts (Port Jefferson, 1992), AIP Conf. Proc. No. 279 (AIP, New York, 1993), p. 197.

[11] C. K. Ng, Phys. Rev. ST Accel. Beams **13**, 121301 (2010).

[12] R. J. England et al., Experiment to Detect Accelerating Modes in a Photonic Bandgap Fiber, in Advanced Accelerator Concepts Workshop (Santa Cruz, 2008), AIP Conf. Proc. No. 1086 (AIP, New York, 2009), p. 550.

[13] B. Kuhlmey, CUDOS MOF Utilities for Micro-Structured Optical Fibres, University of Sydney, Australia. [http://sydney.edu.au/science/physics/cudos/research/mofsoftware.shtml].

[14] BandSolve photonics software, RSoft Design Group, Ossining, NY [www.rsoftdesign.com].

[15] T.P. White et al, Multipole method for microstructured optical fibers I. Formulation, J. Opt. Soc. Am. B, Vol. 19(10), 2322-2330 (2002). B.T. Kuhlmey et al, Multipole method for microstructured optical fibers, II. Implementation and results, J. Opt. Soc. Am. B, Vol. 19(10), 2331-2340 (2002).

[16] K. Leung and Y. Liu, Phys. Rev. Lett. **65**, 2646 (1990).

[17] J. E. Spencer, Int. J. Mod. Phys. A **18**, 2903 (2003).

[18] Incom, Inc., 294 Southbridge Road, Charlton, MA 01507 [http://incomusa.com/].

[19] P. J. Roberts et al, Optics Express **13**, 236 (2005).

[20] G. A. Thomas et al, Nature **404**, 262 (2000).

[21] C. M. Smith et al, Nature **424**, 657 (2003).

[22] D. C. Allan et al, in Photonic Crystal Materials and Devices, A. Adibi, A. Scherer, and S.Y. Lin, eds. Proc. SPIE **5000**, 161 (2003).

[23] M. J. F. Digonnet et al, J. Lightwave Technology **23**, 4169 (2005).

[24] R. J. Noble et al, Designing Photonic Bandgap Fibers for Particle Acceleration, in Proceedings of the 2007 Particle Accelerator Conference (IEEE, Albuquerque, New Mexico, 2007), p. 3101.

[25] R. D. Meade et al, Phys. Rev. B **44**, 10961 (1991).

[26] F. Ramos-Mendieta and P. Halevi, Phys. Rev. B **59**, 15112 (1999).

[27] J. A. West et al, Optics Express **12**, 1485 (2004).

[28] H. K. Kim et al, IEEE J. Quantum Electronics **40**, 551 (2004).

[29] NKT Photonics, photonic band-gap fibers online catalog [http://www.nktphotonics.com].